Theory of the "Forbidden" (222) Electron Reflection in the Diamond Structure

R. D. HEIDENREICH
Bell Telephone Laboratories, Murray Hill, New Jersey
(Received September 16, 1949)

The dynamical or wave-mechanical theory of electron diffraction is extended to include several diffracted beams. In the Brillouin zone scheme this is equivalent to terminating the incident crystal wave vector at or near a zone edge or corner. The problem is then one of determining the energy levels and wave functions in the neighborhood of a corner. The solution of the Schrödinger equation near a zone corner is a linear combination of Bloch functions in which the wave vectors are determined by the boundary conditions and the requirement that the total energy be fixed. This leads to a multiplicity of wave vectors for each diffracted beam giving rise to interference phenomena and is an essential feature of the dynamical theory.

At a Brillouin zone edge formed by boundaries associated with reciprocal lattice points S and G, the orthogonality of the unperturbed wave functions in conjunction with the periodic potential requires that another reciprocal lattice point λ be included in the calculation. The indices of λ must be such that $(\lambda_1\lambda_2\lambda_3)=(s_1s_2s_3)-(g_1g_2g_3)$. The perturbation at the zone edge results in non-zero amplitude coefficients Cg, Cs, and $C\lambda$ for the diffracted waves irrespective of whether or not the structure factor for λ, s or g vanishes. This is the basis of the explanation of the (222) reflection and since it arises through perturbation at a Brillouin zone edge or corner, the term "perturbation reflection" is advanced to replace the commonly used "forbidden reflection."

The octahedron formed by the (222) Brillouin zone boundaries exhibits an array of lines due to intersections with other boundaries to form edges. This array of lines is called a "perturbation grid" and the condition for the occurence of a (222) reflection is simply that the incident wave vector terminate on or near a grid line. Numerical intensity calculations are presented which show that a strong (222) can be accounted for by the dynamical theory.

An impedance network model is briefly discussed which may aid in qualitative considerations of the dynamical theory for the case of several diffracted waves.

INTRODUCTION

SINCE the discovery of electron diffraction some twenty years ago a number of examples of the occurrence of "forbidden" Bragg reflections have been reported. This, of course, has also been true for x-ray diffraction although not to the extent found in electron diffraction. An outstanding example has been the occurrence of a relatively strong (222) reflection from elements crystallizing with the diamond structure. It is the purpose of this paper to show that on the basis of the dynamical theory a (222) reflection is to be expected from diamond.

The term "forbidden" has generally been used to denote the appearance of Bragg reflections for which the structure factor is zero, thus leading to a zero intensity on the basis of the kinematic theory of diffraction. On the basis of the more general, dynamical theory, however, the term "forbidden" as applied to a reflection associated with a zero structure factor is not correct in the sense that zero intensity is no longer predicted. As will be seen, the term "perturbation reflection" would be a more accurate description applicable to the case of a zero structure factor in the dynamical theory.

It is perhaps advisable to consider very briefly the kinematic theory of diffraction and then mention some of the attempts to account for a perturbation reflection using the simple theory. The kinematic theory is actually a first-order approximation to the dynamical theory and amounts to assuming that the various diffracted and transmitted waves in a crystal are completely independent, i.e., no interactions. This approximation does not arise through the use of the Ewald construction in reciprocal space. The Ewald construction is a perfectly general method of predicting the *directions* of diffracted beams and is shown in Fig. 1; the approximation arises in the calculation of the intensities of these beams. The kinematic theory assumes that the amplitude of a wavelet scattered by an infinitesimal volume $dxdydz$ of the crystal is proportional to $Vdxdydz$ where V is the potential inside $dxdydz$. The amplitude of the wave scattered by the entire crystal in the direction RG is then

$$S=\int\int\int V(x,y,z)e^{2\pi i(g\cdot r)}dxdydz;$$

$$(g\cdot r)=g_1x+g_2y+g_3z, \quad (1)$$

with the integral being over the whole crystal. If V is expressed as a Fourier integral,

$$V=\int\int\int_{-\infty}^{+\infty} v_p e^{2\pi i(p\cdot r)}dp_1dp_2dp_3,$$

with $v_p=v_{p_1p_2p_3}$ and $(p\cdot r)=p_1x+p_2y+p_3z$, the scattered amplitude becomes

$$S=\int\int\int\left\{\int\int\int_{-\infty}^{+\infty} v_p e^{2\pi i(p\cdot r)}dp_1dp_2dp_3\right\}$$

$$\times e^{2\pi i(g\cdot r)}dxdydz. \quad (2)$$

In (2), the only terms of consequence are those for which the exponents vanish or $(p\cdot r)=-(g\cdot r)$ which requires that $g_1=-p_1$, $g_2=-p_2$, and $g_3=-p_3$. The amplitude S thus becomes proportional to v_p,

the Fourier coefficient of potential, and the intensity proportional to $|v_p|^2$. When the Ewald sphere touches some other reciprocal lattice point, say Q, the kinematic theory assumes that the intensities of the two beams are independent and are proportional to $|v_p|^2$ and $|v_q|^2$, respectively. As will be seen, this is not so in the dynamical theory where the weight of a reciprocal lattice point such as g is influenced by other points Q, etc., lying near or on the Ewald sphere.

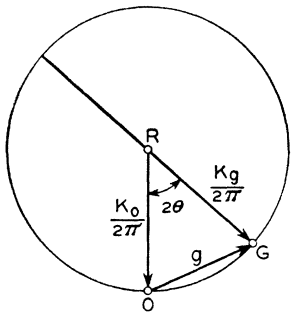

FIG. 1. Ewald construction in reciprocal space for diffracted wave vector. $K_0/2\pi=OR$ is incident crystal wave vector. Sphere of radius $|K_0/2\pi|$ centered at R touches reciprocal lattice point G giving rise to diffracted wave vector $K_g/2\pi=K_0+2\pi g/2\pi=RG$. If $|K_0|^2=|K_g|^2$, the Laue condition is fulfilled. θ is the Bragg angle. The plane of the paper can be viewed as a section through the Ewald sphere where it touches the reciprocal lattice point G so that K_0 and K_g are projected wave vectors.

It would appear at first sight that the interaction among reciprocal lattice points near or touching the Ewald sphere would be of the nature of a minor correction to the kinematic theory and not likely to produce a large effect. That a large correction to the kinematic theory is necessary is demonstrated in the electron diffraction patterns of Fig. 2. Figure 2(a) shows a very strong (222) Laue spot in the pattern from a single crystal of silicon. Over a narrow range of orientation, the (222) is the strongest reflection in the pattern. Figure 2(b) shows a Debye-Scherrer pattern obtained from an evaporated germanium film illustrating the high average intensity of the (222) ring. Figure 2(c) is a reflection pattern from a ground germanium surface in which the crystal size is sufficiently large to produce grainy rings. Local variations in the (222) intensity due to favorably oriented crystallites can be seen. From these and other patterns it is evident that any theory of the (222) reflection must account for a reasonably high intensity. It turns out that the interactions in the dynamical theory can be likened to resonance with coupled oscillators which may produce large responses even though the interaction or coupling is a first-order correction.

The (222) reflection in diamond (and other forbidden reflections) can be viewed as a result of a multiple reflection process. For example, a $(22\bar{2})$ could be considered as compounded from a $(11\bar{3})$ and a $(\bar{1}\bar{1}1)$. In general, compound reflections are those of indices (hkl) arising through diffracted beams of indices $(h_1k_1l_1)$, $(h_2k_2l_2)$ such that $h=h_2-h_1$, $k=k_2-k_1$, and $l=l_2-l_1$. This coupling or interaction condition relating the indices of primary and secondary reflections (to be considered here in detail) was recognized by Renninger[a] and used by him to explain observed (222) and (002) x-ray reflections in diamond. Renninger's conclusions are about the same as those arrived at in this paper, but the general treatment to be given here is considerably different and is based on the concept of Brillouin zones and perturbation of the energy levels at a zone corner. Raether[1] early attributed the forbidden (005) reflection observed in electron diffraction patterns of pyrites to dynamical coupling. Numerous other examples appear in the literature.

An alternative to the above discussion is the possibility that the accepted diamond lattice is not correct and that the structure factor is not zero for the (222). This alternative would seem preferable to the compound reflection theory in some cases. A weak (222) has been observed in x-ray patterns of diamond single crystals although apparently not from all crystals examined and is attributed to the configuration of the valence electrons. A (222) ring has not to the knowledge of the author been found in x-ray powder patterns of diamond, silicon, or germanium. However, this can be interpreted to mean that insufficient path length is available to build up the intensity as required in the dynamical theory. The contribution of the valence electrons to the electron scattering process is likely very small and not capable of accounting for the large intensities observed experimentally.

The conclusion would seem to be that a satisfactory explanation must be found in the dynamical theory. It has been demonstrated[2,3] that the wave-mechanical theory of electron diffraction is approximately correct and capable of explaining in a straightforward manner many experimental observations. The remainder of this paper will be concerned with demonstrating the capabilities of the theory.

I. GENERAL FORMULATION

Although the dynamical theory of electron diffraction has been developed[2] in terms of Brillouin zones, and the calculations carried out in detail for the simple case of a single diffracted wave, it seems

[a] M. Renninger, Zeits. f. Physik **106**, 141 (1937).
[1] H. Raether, Zeits. f. Physik **78**, 527 (1932).
[2] R. D. Heidenreich, J. App. Phys. **20**, 993 (1949).
[3] R. D. Heidenreich and L. Sturkey, J. App. Phys. **16**, 97 (1945). References to earlier work will be found in footnotes 1 and 2.

advisable to briefly state the problem and develop the general theory.

The problem to be considered here (the Laue case) assumes a slab of perfect crystal the front face of which is the x–y plane (Fig. 3). Incident from the left upon the front face is a monochromatic plane vacuum wave, $\varphi_v = A \exp[i(K_v \cdot r)]$, at approximately normal incidence. Inside the crystal the wave function is a linear combination of the various reflected and transmitted waves consistent with the total energy. At the back face, the crystal waves join up with vacuum transmitted and reflected waves. It is assumed that all waves travel in the positive direction of the z axis so that no reflected beams enter the vacuum from the front face.

Before undertaking the mathematical analysis, it is worth while to summarize the pertinent results of the mathematics to aid in understanding the fundamental features of the dynamical theory and to indicate the direction of the calculations. Since the kinematic theory is the first-order approximation to the dynamical theory, it is convenient to begin with the simplest case and show its relation to the more general one. This can be demonstrated schematically by considering the wave vectors in reciprocal space as shown in Fig. 4. In each illustration the wave vectors at the incident vacuum side, the crystal interior, and the exit vacuum side are shown. The incident vacuum wave vector K_v ($|K_v| = 2\pi/\lambda$) is the same in each case. If the crystal is oriented such that the Bragg condition is not realized for any crystal plane and if the inner potential is neglected, then there will be an incident crystal wave vector K_0 and a transmitted wave vector K_t, both of which are the same as K_v as shown in Fig. 4(a). If the incident vacuum wave is a plane wave, then the crystal wave and the transmitted wave are also plane waves joining at the crystal-vacuum surfaces. If now the incident crystal wave vector K_0 terminates on or near a Brillouin zone boundary, there will be a diffracted wave vector $K_g = K_0 + 2\pi g$ which can be drawn in either of the ways shown in Fig. 4(b). There is a transmitted vacuum and diffracted vacuum wave in this case. Figure 4(b) represents the kinematic case in which the waves are still plane waves. If K_0 has its terminus on the Brillouin zone boundary, then the Laue condition $|K_0|^2 = |K_g|^2$ is realized.

As will be seen later, the crystal waves which are solutions of the Schrödinger equation for the periodic potential inside the crystal are Bloch functions which have the form

$$\varphi_j = \sum_l C_l^j \exp[i(K_l^j \cdot r)],$$

with $K_l^j = K_0^j + 2\pi l$ and C_l^j the amplitude coefficient. When K_0 terminates on a Brillouin zone boundary, it turns out that the wave function inside the crystal is a linear combination of two Bloch functions φ_0 and φ_1. There are consequently two incident crystal wave vectors K_0^0 and K_0^1 and two diffracted wave vectors K_g^0 and K_g^1 since φ_0 and φ_1 must have the same energy. K_0^0 and K_g^0 form one Bloch function while K_0^1 and K_g^1 form the other. The boundary conditions require that the crystal wave vectors have tangential components which are equal to that of the incident vacuum wave vector or differ from it by the tangential component of a reciprocal lattice vector. Consequently, K_0^0 and K_0^1 have equal tangential components as do K_g^0 and K_g^1 with the normal components differing by a vector ΔK normal to

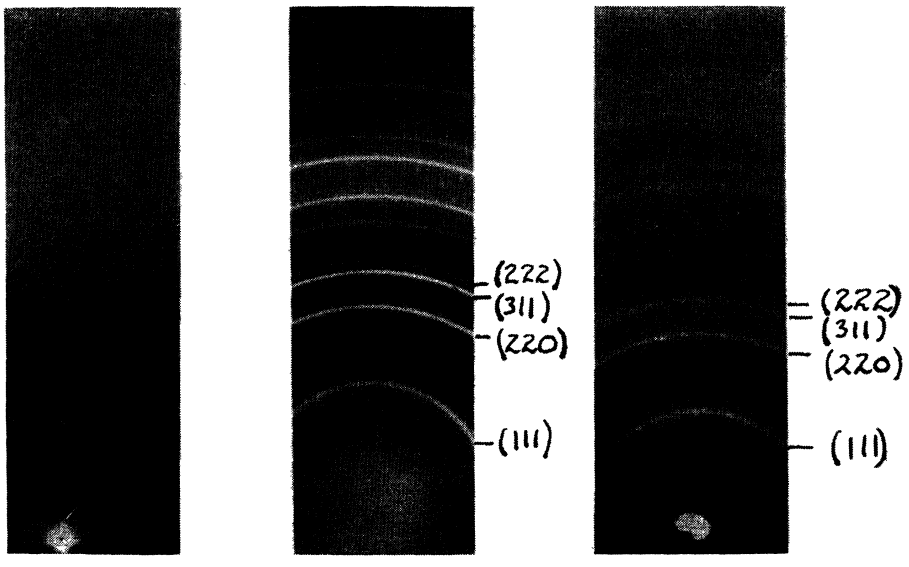

FIG. 2. Examples of the "forbidden" (222) reflection in electron diffraction patterns from silicon and germanium (40-kv electrons). (a) Strong (222) Laue spot from an etched single crystal of silicon. (Courtesy of K. H. Storks.) (b) Transmission pattern from an evaporated germanium film on a silica substrate. (c) Reflection pattern from a ground germanium surface showing grainy rings.

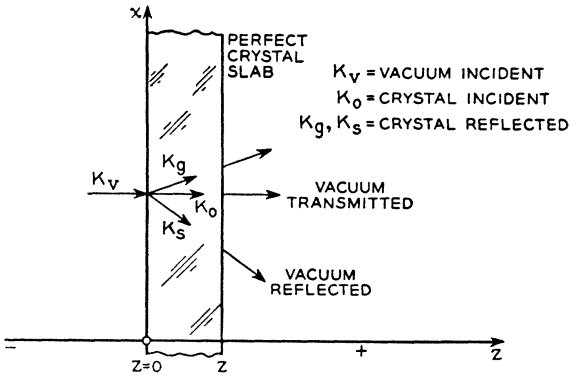

FIG. 3. Representation of the Laue case of the dynamical theory where no radiation emerges from same surface into which it enters. Electrons are incident from the left onto the front surface of a crystal slab bounded by the planes $z=0$ and $z=z$. The various transmitted and diffracted wave vectors are shown. In the case to be considered in detail, K_0 is approximately along the [1$\bar{1}$0] crystal axis of germanium (Fig. 6).

the surface as shown in Fig. 4(c). K_g^0 and K_g^1 are out of phase at the incident surface so that the amplitude of the diffracted wave is zero at the surface and increases with penetration into the crystal.

The essential feature of the dynamical theory is the multiplicity of wave vectors such as K_g^0 and K_g^1 associated with a single diffracted wave. It is here that the interference phenomena arise with ΔK being the beat wave vector. The multiplicity of diffracted wave vectors can be viewed as multiple refraction (the crystal is doubly refracting in the case of Fig. 4(c)).

The extension to any number of diffracted waves is evident. The incident crystal wave vector may terminate at a Brillouin zone edge or corner and give rise to several diffracted waves. At a zone edge, however, formed by reciprocal lattice points S and G (Fig. 4(c)), the mathematics require that another reciprocal lattice point λ be considered. The indices of λ must be such that

$$(\lambda_1\lambda_2\lambda_3)=(s_1s_2s_3)-(g_1g_2g_3).$$

The solution in the crystal for this case consists of four Bloch functions with the same energy and hence four wave vectors for the transmitted and each diffracted beam. There will now be three distinct beat wave vectors as shown in Fig. 4(d). Of particular interest is the case when the structure factor associated with one of the reciprocal lattice points S, G, or λ is zero. If the structure factor for S vanishes, it turns out that the amplitude coefficients C_s^i do not vanish and may be comparable to C_g^i, for example. Thus, at a zone corner it is possible to produce a diffracted beam corresponding to a zero structure factor. This is the basis of the theory of the (222) reflection to be advanced. The following sections are concerned with the mathematical analysis leading to the calculation of intensities. The procedure is that commonly used in perturbation theory and is concerned with determining the energy levels at a corner, the amplitude coefficients, and finally the intensities.

A. Crystal Wave Functions

The general motion of an electron of total energy E in a region where the potential is $V(x, y, z)$ is described by the Schrödinger equation,

$$H\varphi=E\varphi \text{ with } H\equiv-\frac{h^2}{8\pi^2m}\nabla^2+V(x,y,z).$$

In a perfect crystal, the potential can be repre-

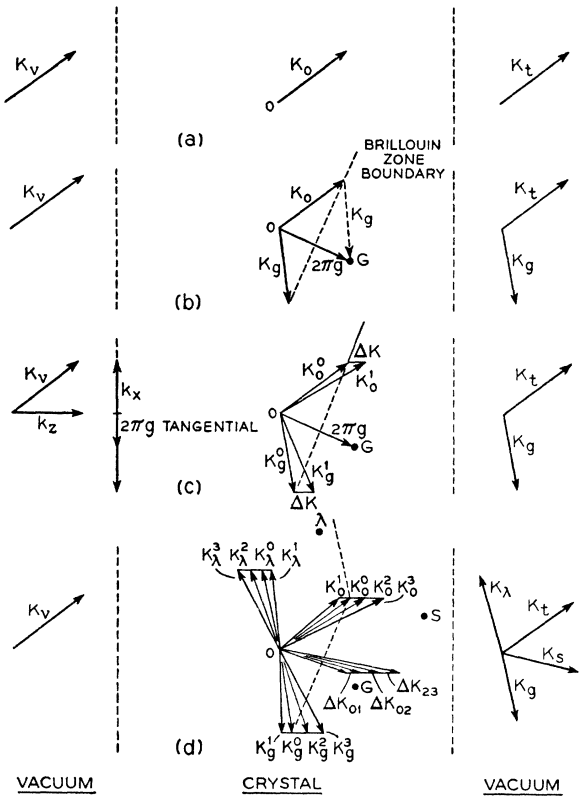

FIG. 4. Relations among wave vectors in reciprocal space for several approximations in diffraction theory. The representation may be taken as projections of the vectors onto the plane of the paper. The incident plane wave is from the left and the emergent plane waves on the right. (a) Zero approximation. No interaction with crystal. (b) Kinematic or first approximation. Single diffracted wave vector $K_g=K_0+2\pi g$. The diffracted wave in the crystal is a single plane wave. (c) Dynamical theory, single diffracted beam. The diffracted wave in the crystal now consists of two plane waves with wave vectors K_g^0 and K_g^1. The wave function in the crystal is a linear combination of two Bloch waves, one with wave vectors K_0^0 and K_g^0 and the other width K_0^1 and K_g^1. The boundary requirement for the tangential components is shown. (d) Dynamical theory, three diffracted beams (Brillouin zone edge). The structure factor of any one of the three reflections may be zero and still give rise to a non-zero amplitude for that reflection. (In (c) and (d), the beat wave vectors. ΔK, are normal to the crystal surface.)

sented by a Fourier series[b]

$$V(x, y, z) = -(V_0 + \sum_g{}' v_g e^{2\pi i(g\cdot r)}), \quad (4)$$

where $g = g_1 b_1 + g_2 b_2 + g_3 b_3$ is a reciprocal lattice vector and $v_g \equiv v_{g_1 g_2 g_3}$ for brevity. The prime on the summation over the triple indices means that $g_1 = g_2 = g_3 = 0$ is excluded since it is written as V_0 (the inner potential).

In field-free space, $V = V_0$, the solution of the equation

$$H^{(0)}\varphi_j^{(0)} = E_j^{(0)}\varphi_j^{(0)} \text{ with } H^{(0)} \equiv \frac{-h^2}{8\pi^2 m}\nabla^2 + V_0 \quad (5)$$

is a superposition of plane waves. Assume that the solution of (3) can be expanded in terms of the unperturbed wave functions φ_j^0 of (5) or

$$\varphi = \sum_j c_j \varphi_j^{(0)}, \quad (6)$$

with the c_j's to be determined. Substituting (6) into (3) and using (5) obtain

$$\sum_j (V\varphi_j^{(0)} + \beta_j \varphi_j^{(0)}) C_j = 0, \quad (7)$$

where $\beta_j = (E_j^{(0)} - E)$ and

$$E_j^{(0)} = h^2 |K_j|^2 / 8\pi^2 m.$$

Multiplying (7) on the left by $\varphi_m{}^{0*}$ (the complex conjugate of $\varphi_m{}^0$) and integrating over the unit cell, Ω,

$$\sum_j \left\{ \int_\Omega \varphi_m{}^{(0)*} V \varphi_j^{(0)} d\gamma + \beta_j \int_\Omega \varphi_m{}^{(0)*} \varphi_j^{(0)} d\gamma \right\} C_j = 0. \quad (8a)$$

If the expression (4) for the potential is placed in (8a) and if the subscripts j and m of (8a) are identified with reciprocal lattice vectors,[c] there is obtained upon integration

$$\beta_m C_m = \sum_{j,\, j \neq m} v_{m-j} \cdot C_j. \quad (8b)$$

The Fourier coefficient v_{m-j} occurs in (8b) as a result of the orthogonality of the unperturbed wave functions $\varphi_j^{(0)}$. Equation (8b) is the desired relation between the amplitude coefficients, the Fourier coefficients and the energy and is sometimes called the "dispersion equation." In (8b),

$$\beta_j \equiv \left(\frac{h^2 |K_j|^2}{8\pi^2 m} - E \right)$$

rather than $[|K_j|^2 - (8\pi^2 m/h^2)E]$ as employed in reference 2.

Suppose now that the Ewald sphere passes in the neighborhood of reciprocal lattice points g and s. In (8b), j and m then take on the values, 0, g, and s. The Fourier coefficient v_{m-j} will take on not only the values v_g, $v_{-g}{}^*$, v_s, $v_s{}^*$ but also v_{s-g} and $v_{s-g}{}^*$. If $\lambda = s - g$, C_λ must be taken into account if the reciprocal lattice point λ lies near the Ewald sphere. The set of Eqs. (8) for the case of amplitudes C_0, C_g, C_s, and C_λ with $\lambda = s - g$ then becomes

$$\begin{bmatrix} \beta_0 & -v_g{}^* & -v_s{}^* & -v_\lambda{}^* \\ -v_g & \beta_g & -v_\lambda{}^* & -v_{\lambda-g}{}^* \\ -v_s & -v_\lambda & \beta_s & -v_g \\ -v_\lambda & -v_{\lambda-g} & -v_g{}^* & \beta_\lambda \end{bmatrix} \begin{Bmatrix} C_0 \\ C_g \\ C_s \\ C_\lambda \end{Bmatrix} = 0. \quad (9)$$

The roots of the secular determinant[d] of (9) are the eigenvalues from which the possible crystal wave vectors and energy gaps are determined. The amplitude coefficients C_g, C_s, C_λ are obtained from (9) in terms of C_0, the Fourier coefficients and the eigenvalues. The solution is thus a one-electron Bloch function reducing to a plane wave when the Fourier coefficients of potential approach zero.

There will be one Bloch function for each root of the secular determinant (9) which, for a given K_0, will have different energies corresponding to the different roots. It is possible to choose a set of distinct vectors $K_0{}^0$, $K_0{}^1$, $K_0{}^2$, and $K_0{}^3$ (one for each root of the secular determinant) which have the same tangential components as the incident vacuum wave vector and correspond to the same total energy. (The total energy is fixed in a diffraction experiment.) With the tangential components fixed, the normal components are adjusted to satisfy the requirement for fixed E so that $K_0{}^1$, for example, can be written

$$K_0{}^1 = K_0{}^0 + \Delta K_{01},$$

where ΔK_{01} is normal to the surface. The various wave vectors and ΔK's are illustrated in Fig. 4(d).

A Bloch solution exists for each allowed wave vector $K_0{}^0$, $K_0{}^1$, etc., so that the possible solutions are

$$\begin{aligned} \varphi_0 &= \sum_{p=0,\, g,\, s,\, \lambda} C_p{}^0 \exp[i(K_p{}^0 \cdot r)], \\ &\cdot \\ &\cdot \\ \varphi_3 &= \sum_{p=0,\, g,\, s,\, \lambda} C_p{}^3 \exp[i(K_p{}^3 \cdot r)] \end{aligned} \quad (10)$$

and the crystal wave function is a linear combination of such solutions

$$\psi_c = a_0\varphi_0 + a_1\varphi_1 + a_2\varphi_2 + a_3\varphi_3, \quad (11)$$

where the a's are coefficients to be determined by the boundary conditions.

[b] Reference 1, Appendix I.

[c] If K_0 denotes the incident wave vector and m a reciprocal lattice vector, then $K_m = K_0 + 2\pi m$ is a diffracted wave vector.

[d] The matrix in (9) is Hermitian and hence the secular determinant possesses four real roots.

From the linear combination of Bloch functions (11), the transmitted and diffracted waves associated with K_0^0, K_0^1, K_0^2 and K_0^3 can be sorted out according to the subscripts and written separately as

$$\begin{aligned}\zeta_t &= \sum_{l=0,1,2,3} a_l C_0{}^l \exp[i(K_0{}^l\cdot r)],\\ &\cdots\cdots\cdots\cdots\\ \zeta_\lambda &= \sum_{l=0,1,2,3} a_l C_\lambda{}^l \exp[i(K_\lambda{}^l\cdot r)].\end{aligned} \tag{12}$$

Here ζ_t is the transmitted wave amplitude and ζ_g, ζ_s, ζ_λ are diffracted amplitudes. In this case a diffracted wave, say ζ_g, is now characterized by four wave vectors (Fig. 4(d)) rather than the single one of the kinematic theory, and consists of a series of terms, one from each Bloch function.

The amplitude coefficients, a, in Eq. (12) are determined by the boundary conditions at the incident crystal surface ($z=0$). If $A\exp[i(K_v\cdot r)]$ denotes the incident plane wave, then the following equations apply at $z=0$.

$$\begin{Bmatrix} C_0{}^0 & C_0{}^1 & C_0{}^2 & C_0{}^3\\ C_g{}^0 & C_g{}^1 & C_g{}^2 & C_g{}^3\\ C_s{}^0 & C_s{}^1 & C_s{}^2 & C_s{}^3\\ C_\lambda{}^0 & C_\lambda{}^1 & C_\lambda{}^2 & C_\lambda{}^3 \end{Bmatrix} \begin{Bmatrix} a_0\\ a_1\\ a_2\\ a_3 \end{Bmatrix} = \begin{Bmatrix} A\\ 0\\ 0\\ 0 \end{Bmatrix}. \tag{13}$$

Equations (13) are immediately obtained from (12) at $z=0$ where $\zeta_t=A$ and $\zeta_g=\zeta_s=\zeta_\lambda=0$. The exponentials do not occur since the tangential components of all wave vectors are equal or differ by a reciprocal lattice vector at $z=0$. The same boundary conditions apply at the exit surface but need not be considered since all the coefficients and amplitudes are determined at the incident surface and by the potential inside the crystal.

B. Intensities

Having obtained explicit wave functions (12) for the transmitted and diffracted beams, the calculation of the intensities is straightforward. If I_n is the intensity associated with the indices n, then

$$\begin{aligned} I_n &= \zeta_n\zeta_n{}^*\\ &= \sum_{l,s=0,1,2,3} \{a_l a_s{}^* C_n{}^l C_n{}^{s*} \exp[i(K_n{}^l - K_n{}^s)\cdot r]\\ &\quad + a_l{}^* a_s C_n{}^{l*} C_n{}^s \exp[-i(K_n{}^l - K_n{}^s)\cdot r]\}. \end{aligned} \tag{14a}$$

Since the coefficients of the exponentials are complex conjugates, the intensity is real and (14a) can be simplified and written

$$\begin{aligned} I_n &= |a_0 C_n{}^0 + a_1 C_n{}' + a_2 C_n{}^2 + a_3 C_n{}^3|{}^2\\ &\quad - 2\sum_{\substack{l,s=0,1,2,3\\ l\neq s}} a_l a_s{}^* C_n{}^l C_n{}^{s*} \sin^2 \tfrac{1}{2}(k_0{}^l - k_0{}^s)_z z, \end{aligned} \tag{14b}$$

where the term $l=s$ has been removed from the summation and $(k_0{}^l - k_0{}^s)_z$ is the z or normal component of $K_0{}^l - K_0{}^s$.

The fine structure of a Laue spot can be obtained by evaluating the intensities for each of the wave vectors $K_n{}^0$, $K_n{}^1$, etc. The angular spread between $K_n{}^0$ and $K_n{}^1$, etc. is of the order of $\Delta E/E$ where ΔE is the energy gap at the zone boundary and is about 10^{-4} rad. for 40-kv electrons. Such a procedure may be necessary in interpreting diffraction patterns where high resolution is obtained.

The first term on the right of Eq. (14b) vanishes for all but the transmitted beam as seen from (13). The intensity of a diffracted beam thus consist of a sum of $\sin^2$ terms such as is obtained in treating interference phenomena in light optics. The arguments of the $\sin^2$ terms in (14b) can be written $\frac{1}{2}(k_0{}^l - k_0{}^s)_z z = \frac{1}{2}|\Delta K_{sl}|z$ where ΔK_{sl} is determined from the secular roots[e] and is the beat wave number or "anpassung" in Bethe's original theory.[4]

In using (14b) it must be remembered that the following assumptions are incorporated:

(a) A perfect crystal in which the potential is represented by a Fourier series.

(b) An abrupt discontinuity in potential at the crystal-vacuum interface. Laue[5] has shown that this assumption is valid for fast electrons.

(c) No attenuation due to inelastic scattering. The possibility of including inelastic scattering into the dynamical theory using Slater's[6] complex potential method has yet to be investigated.

II. EQUIVALENT CIRCUIT FOR ELECTRON DIFFRACTION

The foregoing discussion is equivalent to an extension of Bethe's treatment,[4] the difference being chiefly one of terminology and the explicit use of energy levels as a means of determining the permissible crystal wave vectors. In the Brillouin zone scheme, the Laue conditions are equivalent to requiring that the incident wave vector, K_0, terminate on a Brillouin zone boundary. The existence of one or more diffracted beams is determined by the details of the energy discontinuities at the zone boundary. A single energy gap allows one and only one diffracted beam and is realized when the terminus of K_0 is not near a zone edge or corner. The multiple energy gap arising in the vicinity of a zone corner gives rise to two or more diffracted beams; in the case of Eq. (9) there will be four energy levels at the corner and three diffracted beams. The number of diffracted beams is always one less than the number of roots of the secular determinant. However, the relative intensities of

[e] For example: If E_0 and E_1 are two of the secular energy roots, then ΔK_{01} is determined by $E_0(K_0{}^0)=E_1(K_0{}^1)=E_1(K_0{}^0+\Delta K_{01})$. $|\Delta K_{01}|^2$ can be neglected as can $(\Delta K_{01}\cdot g)$ for most approximations.

[4] H. A. Bethe, Ann. d. Physik **87**, 55 (1928).

[5] M. von Laue, Phys. Rev. **37**, 53 (1931).

[6] J. C. Slater, Phys. Rev. **51**, 74 (1937).

the possible beams is not simply related to the magnitudes of the energy gaps at the boundary. A detailed calculation is necessary to obtain the intensities as will be demonstrated in a later section. Although the use of Eqs. (9), (13), and (14b) is sufficient to determine the energy levels at a zone corner and the intensities of the diffracted beams, the model is strictly formal and does not appeal to the intuition. For this reason, the use of a coupled oscillator model in the form of an equivalent circuit will be mentioned which presents a relatively simple physical model for the dynamical theory.

The impedance network model for the diffraction problem is obtained directly from the energy matrix (9) for the specific case of a periodic potential and is not as general as that employed by Kron.[7] If the energy matrix (9) is viewed as an electrical network matrix whose meshes contain inductance and capacitance, the off-diagonal terms represent the elastances of the coupling condensers. If the correspondence is carried out it is found that the Fourier coefficients of potential in (9) behave as couplings between the various beams which correspond to the meshes of the network. The condition for resonance between two meshes (identical natural frequencies) is just the Laue condition in the diffraction case.

A network can be drawn for the matrix (9) only if one or more of the Fourier coefficients vanish. If $v_{\lambda-g}=0$, the network is that shown in Fig. 5(a). If $v_\lambda=0$, in addition, where λ might be (222), the network is that shown in Fig. 5(b). Mesh λ is no longer directly coupled to the incident or driver mesh 0 but still may be driven through the coupling condensers v_g and v_s, providing that $\lambda=s-g$. If $\lambda=(222)$, then a possibility is $g=(\bar{1}\bar{1}\bar{1})$ and $s=(113)$. If mesh g is detuned sufficiently that its response can be neglected, the matrix of the system can be reduced in order from four to three. This reduction in order through neglecting the response of one mesh (or beam) greatly facilitates the calculation of intensities when such an approximation is valid as will be seen. No computational advantages are gained from the network analogy unless a network analyzer can be used. A more detailed consideration of the analogy is not justified at this time.

III. (222) INTENSITIES

In order to compute the diffracted intensities, it is necessary to know the details of the reciprocal lattice geometry and the Brillouin zone corners. All the numerical calculations in this paper will be made for germanium ($a_0=5.65$A), but either diamond or silicon would do as well. Since the (222) reflection is of primary interest, it is convenient to consider a plane section of the reciprocal lattice normal to the $[1\bar{1}0]$ zone axis as shown in Fig. 6. The reciprocal lattice points are located to scale and the Brillouin zone boundaries drawn as the perpendicular bisectors of the respective reciprocal lattice vectors.[8] The zone boundaries of interest are parallel to the $[1\bar{1}0]$ crystal axis. The edges influencing the $(22\bar{2})$ reflection are then those such as A, B, C, D of Fig. 6. In the first example to be considered, the incident crystal wave vector, K_0, is drawn from the origin so that it terminates at the $(111)|(22\bar{2})$ zone corner.[f] $K_0{}^p/2\pi$ is the projection of the incident crystal wave vector on the plane of the paper (containing the labeled reciprocal lattice points). The third reciprocal lattice point involved must be such that $\lambda=s-g$. Thus, if $g\equiv(111)$, $s\equiv(22\bar{2})$, then $\lambda=(11\bar{3})$. If a circle of radius $|K_0{}^p/2\pi|$ is drawn with C as center, it will be seen that the reciprocal lattice point $\lambda=(11\bar{3})$ lies some distance off the circle. The point (220) lies somewhat nearer the circle but does not interact since the indices do not satisfy the condition $\lambda=s-g$. Since $(11\bar{3})$ is considerably off from the Laue condition, its amplitude is assumed sufficiently weak that it can be neglected as a first approximation. Neglecting C_λ and setting $v_s=0$ in (9) gives, for point C,

$$\begin{bmatrix} \beta_0 & -v_g{}^* & 0 \\ -v_g & \beta_g & -v_\lambda{}^* \\ 0 & -v_\lambda & \beta_s \end{bmatrix} \begin{Bmatrix} C_0 \\ C_g \\ C_s \end{Bmatrix} = 0. \tag{15}$$

Since $|K_g|^2=|K_s|^2=|K_0|^2$, $\beta_0=\beta_g=\beta_s$, and the

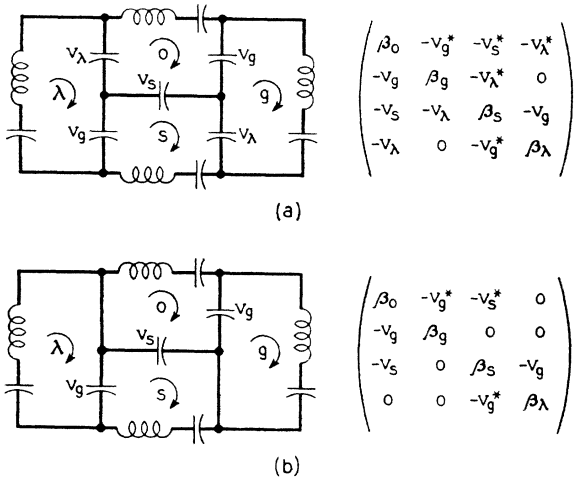

FIG. 5. Equivalent networks for dynamical theory based on the matrix (9) for the periodic potential. (a) $v_{\lambda-g}=0$. (b) $v_{\lambda-g}=v_\lambda=0$. The coupling condensers are labeled with the Fourier coefficients to which they correspond. Mesh 0 is taken to be the "driver." In (b), mesh λ corresponds to the case of the (222) reflection which responds through the couplings v_s and v_g even though not directly coupled to the driver.

[7] G. Kron, Phys. Rev. **67**, 39 (1945).

[8] See L. Brillouin, *Wave Propagation in Periodic Structures* (McGraw-Hill Book Company, Inc., New York, 1946).

[f] The symbol $(h_1k_1l_1)|(h_2k_2l_2)$ will be used to denote the intersection of zone boundaries $(h_1k_1l_1)$ and $(h_2k_2l_2)$.

secular determinant yields the cubic

$$\beta_0^3-\beta_0|v_\lambda|^2-\beta_0|v_g|^2=0, \tag{16}$$

with the roots $\beta_0^0=0$, $\beta_0^1=+(|v_g|^2+|v_\lambda|^2)^{\frac{1}{2}}=+\Delta E$, $\beta_0^2=-(|v_g|^2+|v_\lambda|^2)^{\frac{1}{2}}=-\Delta E$. The energies are then[g]

$$E^0=h^2|K_0|^2/8\pi^2m,$$

$$E^1=\frac{h^2|K_0|^2}{8\pi^2m}-(|v_g|^2+|v_\lambda|^2)^{\frac{1}{2}}=\frac{h^2|K_0|^2}{8\pi^2m}-\Delta E, \tag{17}$$

$$E^2=\frac{h^2|K_0|^2}{8\pi^2m}+(|v_g|^2+|v_\lambda|^2)^{\frac{1}{2}}=\frac{h^2|K_0|^2}{8\pi^2m}+\Delta E.$$

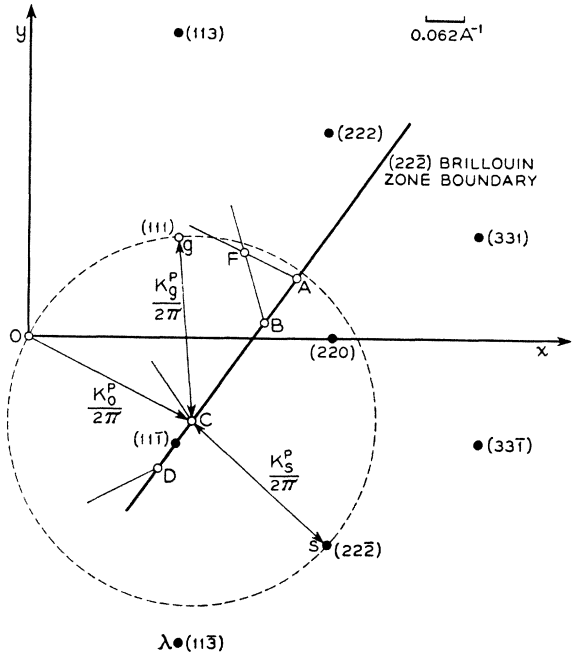

FIG. 6. Plane section through germanium reciprocal lattice drawn to scale with Miller indices of reciprocal lattice points given. The plane of the paper is normal to the [1$\bar{1}$0] crystal axis. Brillouin zone edges A, B, C, and D are all common to the (22$\bar{2}$) zone boundary. $K_0^p/2\pi$ is the projection of the incident crystal wave vector on the plane of the paper and terminates at the (111)|(22$\bar{2}$) corner. The circle of radius $|K_0^p/2\pi|$ passes through reciprocal lattice points (22$\bar{2}$) and (111) but misses (11$\bar{3}$). The edges are as follows

A....(113)|(22$\bar{2}$). Couples with (331).
B....(331)|(22$\bar{2}$). Couples with (113).
C....(111)|(22$\bar{2}$). Couples with (11$\bar{3}$).
D....(11$\bar{3}$)|(22$\bar{2}$). Couples with ($\bar{1}\bar{1}\bar{1}$).
F....(113)|(331). Couples with (22$\bar{2}$).

The permissible incident wave vectors are found by equating the roots (17) with $K_0^1=K_0^0+\Delta K_{01}$, $K_0^2=K_0^0+\Delta K_{02}$ so that[h]

$$\Delta K_{01}\simeq K_0^1-K_0^0\simeq\frac{\Delta E}{2}\frac{8\pi^2m}{h^2K_0}=\frac{\pi\Delta E}{\lambda E^{(0)}},$$

$$\Delta K_{02}\simeq K_0^2-K_0^0\simeq-\frac{\Delta E}{2}\frac{8\pi^2m}{h^2K_0}=-\frac{\pi\Delta E}{\lambda E^{(0)}}, \tag{18}$$

$$\Delta K_{12}\simeq K_0^2-K_0^1\simeq-\Delta E\frac{8\pi^2m}{h^2K_0^0}=-\frac{2\pi\Delta E}{\lambda E^{(0)}}.$$

It is not necessary to calculate the crystal wave functions explicitly when using (14b) to compute the intensities. The boundary Eqs. (13) are for this case ($a_3=0$),

$$\begin{vmatrix} C_0^0 & C_0^1 & C_0^2 \\ C_g^0 & C_g^1 & C_g^2 \\ C_s^0 & C_s^1 & C_s^2 \end{vmatrix}\begin{Bmatrix} a_0 \\ a_1 \\ a_2 \end{Bmatrix}=\begin{Bmatrix} A \\ 0 \\ 0 \end{Bmatrix}.$$

Writing $C_g=\alpha_gC_0$, $C_s=\alpha_sC_0$, etc., the constants a_0, a_1, and a_2 are found to be

$$a_0=A\frac{\alpha_s^1\alpha_g^2-\alpha_s^2\alpha_g^1}{|c|}C_0^1C_0^2;$$

$$a_1=-A\frac{(\alpha_s^0\alpha_g^2-\alpha_s^2\alpha_g^0)}{|c|}C_0^0C_0^2; \tag{19}$$

$$a_2=A\frac{(\alpha_s^0\alpha_g^1-\alpha_s^1\alpha_g^0)}{|c|}C_0^0C_0^1,$$

with

$$|c|=C_0^0C_0^1C_0^2[(\alpha_s^1\alpha_g^2-\alpha_s^2\alpha_g^1)-(\alpha_s^0\alpha_g^2-\alpha_s^2\alpha_g^0)+(\alpha_s^0\alpha_g^1-\alpha_s^1\alpha_g^0)].$$

The α's are easily found from (15) to be

$$\alpha_g=\frac{\beta_sv_g-\beta_0v_\lambda^*}{\beta_s\beta_g-v_\lambda^*(v_g^*+v_\lambda)};\quad \alpha_s=-\frac{\beta_g\beta_0-v_g(v_g^*+v_\lambda)}{\beta_g\beta_s-v_\lambda^*(v_g^*+v_\lambda)}.$$

Since $\beta_0=\beta_g=\beta_s$, there is finally obtained the relations

$$\begin{aligned} &\alpha_g^0=0;\ (\beta_0^0=0), && \alpha_s^0=-v_g/v_\lambda^*,\\ &\alpha_g^1=\beta_0^1/v_g^*, && \alpha_s^1=v_\lambda/v_g^*,\\ &\alpha_g^2=\beta_0^2/v_g^*=-\alpha_g^1, && \alpha_s^2=\alpha_s^1. \end{aligned} \tag{20}$$

By (19) and (20)

$$a_0a_1^*=-\frac{1}{2}\frac{|A|^2}{C_0^0C_0^{1*}}\frac{\alpha_s^1\alpha_s^{0*}}{|\alpha_s^1-\alpha_s^0|^2},$$

$$a_0a_2^*=-\frac{1}{2}\frac{|A|^2}{C_0^0C_0^{2*}}\frac{\alpha_s^1\alpha_s^{0*}}{|\alpha_s^1-\alpha_s^0|^2}, \tag{21}$$

$$a_0a_2^*=+\frac{1}{4}\frac{|A|^2}{C_0^1C_0^{2*}}\frac{|\alpha_s^0|^2}{|\alpha_s^1-\alpha_s^0|^2},$$

with $\alpha_0^*\alpha_1=(\alpha_0\alpha_1^*)^*$ etc. The relative intensities

[g] Since $\beta_0\equiv[(h^2|K_0|^2/8\pi^2m)-E]\equiv[E^{(0)}-E]$.

[h] The approximation $(\Delta K\cdot K)\cong|\Delta K||K|$ is employed for the case of nearly normal incidence where the direction cosines of the incident wave vector is nearly unity. Otherwise, the expressions (18) will contain the direction cosines in the denominator.

are found from (14b) to be

$$I_{(22\bar{2})}=\frac{|\alpha_s{}^1|^2|\alpha_s{}^0|^2}{|\alpha_s{}^1-\alpha_s{}^0|^2}[4\sin^2\tfrac{1}{2}(\Delta K_{01}z)-\sin^2\tfrac{1}{2}(\Delta K_{12}z)],$$

$$I_{(111)}=\frac{|\alpha_g{}^1|^2|\alpha_s{}^0|^2}{|\alpha_s{}^1-\alpha_s{}^0|^2}\sin^2\tfrac{1}{2}(\Delta K_{12}z), \tag{22a}$$

$$I_t=1+\frac{2(\alpha_s{}^1\alpha_s{}^{0*}+\alpha_s{}^{1*}\alpha_s{}^0)}{|\alpha_s{}^1-\alpha_s{}^0|^2}\sin^2\tfrac{1}{2}(\Delta K_{01}z)-\frac{|\alpha_s{}^0|^2}{|\alpha_s{}^1-\alpha_s{}^0|^2}\sin^2\tfrac{1}{2}(\Delta K_{12}z).$$

Introducing numerical values for the Fourier coefficients (Appendix I), the final result is

$$\begin{aligned}I_{(22\bar{2})}&=0.23[4\sin^2\pi z/z_0-\sin^2\pi 2z/z_0],\\ I_{(111)}&=0.59\sin^2\pi 2z/z_0,\\ I_t&=1-0.90\sin^2\pi z/z_0-0.37\sin^2\pi 2z/z_0,\end{aligned} \tag{22b}$$

where, by (18),

$$z_0=\frac{2\lambda E^{(0)}}{\Delta E}(\Delta E=(|v_g|^2+|v_\lambda|^2)^{\frac{1}{2}}=10.5\text{ volts}).$$

Figure 7 shows a plot of the intensities (22b) as a function of penetration in the crystal, z, for 40-kv electrons ($\lambda=0.061$A). The intensities averaged over thickness or path length in the crystal are found by setting $\sin^2=\frac{1}{2}$ in (22b) or $\langle I_{(111)}\rangle_{Av}=0.30$ and $\langle I_{(22\bar{2})}\rangle_{Av}=0.32$. Hence, not only is there a $(22\bar{2})$ reflection at the $(111)|(22\bar{2})$ zone corner, but the intensity is about the same as that of the (111) intensity. It will be noted that the intensity of the reflection builds up more slowly than does that of the allowed reflection.

The energy as a function of wave vector along the vector K_0 to $(111)|(22\bar{2})$ is of interest. Returning to (15) with $\beta_0\neq\beta_g\neq\beta_s$ and writing $\beta_g=\beta_0+\Delta_g$ and $\beta_s=\beta_0+\Delta_s$ where

$$\Delta_g\equiv(h^2/8\pi^2m)(|K_g|^2-|K_0|^2)$$

and

$$\Delta_s\equiv(h^2/8\pi^2m)(|K_s|^2-|K_0|^2)$$

the secular determinant is ($g\equiv(111)$, $s\equiv(22\bar{2})$, $\lambda\equiv(11\bar{3})$ as before)

$$\begin{vmatrix}\beta_0 & -v_g^* & 0\\ -v_g & \beta_0+\Delta_g & -v_\lambda^*\\ 0 & -v_\lambda & \beta_0+\Delta_s\end{vmatrix}=0 \tag{23}$$

yielding a cubic. The roots are most conveniently evaluated by numerical calculation for various values of $|K_0|^2$. The deviations, Δ_g and Δ_s, can be found from Fig. 6 by measuring the projections of K_0, K_g, and K_s and computing the differences of the squares. The energies so obtained are in the form of that for a free electron, $E^{(0)}=h^2|K_0|^2/8\pi^2m$, plus a correction term. Two of the roots possess a positive correction and one a negative correction. A plot of energy *versus* wave number along K_0 is shown in Fig. 8 using the reduced zone scheme.

If the amplitude coefficient C_λ ($\lambda\equiv(11\bar{3})$) had not been neglected, the secular determinant at point C would have been

$$\begin{vmatrix}\beta_0 & -v_g^* & 0 & -v_\lambda^*\\ -v_g & \beta_g & -v_\lambda^* & -v_{\lambda-g}^*\\ 0 & -v_\lambda & \beta_s & -v_g\\ -v_\lambda & -v_{\lambda-g} & -v_g^* & \beta_\lambda\end{vmatrix} \tag{24}$$

rather than (23). The Fourier coefficient $v_{\lambda-g}=v_{(00\bar{4})}$ now occurs as a coupling between meshes g and λ. The plot of energy *vs.* wave number $|K_0|$ (along K_0) to the corner will now appear as in Fig. 9 as compared to Fig. 8. The retention of C_λ has increased the perturbation.

The cubic approximation demonstrated for point C of Fig. 6 can be applied at corners A, B, and D along the $(22\bar{2})$ zone boundary. The intensities obtained at corners A, B, and D are as follows:

Corner A: $(113)|(22\bar{2})$;
$s\equiv(331)$; $g\equiv(113)$; $\lambda=(22\bar{2})$; $v_{\lambda-g}=v_{11\bar{5}}$.
C_{331} neglected: $\Delta E=(|v_g|^2+|v_{\lambda-g}|^2)^{\frac{1}{2}}=7$ volts.
$I_{(22\bar{2})}=0.14[4\sin^2\pi z/z_0-\sin^2\pi 2z/z_0]$;
$z_0=2\lambda E/\Delta E=700$A,
$I_{(113)}=0.93\sin^2\pi 2z/z_0$,
$I_t=1-0.56\sin^2\pi z/z_0-0.76\sin^2\pi 2z/z_0$,
$\langle I_{(22\bar{2})}\rangle_{Av}=0.21$; $\langle I_{(113)}\rangle_{Av}=0.46$.

Corner B: $(331)|(222)$;
$s\equiv(331)$, $g\equiv(113)$, $\lambda=(22\bar{2})$.
C_{113} neglected; $\Delta E=(|v_g|^2+|v_s|^2)^{\frac{1}{2}}=7.3$ volts.
$I_{(222)}=0.17[4\sin^2\pi z/z_0-\sin^2\pi 2z/z_0]$,
$I_{(331)}=0.24\sin^2\pi 2z/z_0$,
$I_t=1-0.68\sin^2\pi z/z_0-0.06\sin^2\pi 2z/z_0$,
$\langle I_{(22\bar{2})}\rangle_{Av}=0.27$; $\langle I_{(331)}\rangle_{Av}=0.11$.

Corner D: $(11\bar{3})|(22\bar{2})$;
$s\equiv(11\bar{3})$, $g\equiv(\bar{1}11)$, $\lambda=(22\bar{2})$.
$C_{(111)}$ neglected: $\Delta E=(|v_g|^2+|v_s|^2)^{\frac{1}{2}}=10.7$ volts.
$I_{(22\bar{2})}=0.23[4\sin^2\pi z/z_0-\sin^2\pi 2z/z_0]$; $z_0=450$A,
$I_{(11\bar{3})}=0.36\sin^2\pi 2z/z_0$,
$I_t=1-0.93\sin^2\pi z/z_0-0.13\sin^2\pi 2z/z_0$,
$\langle I_{(22\bar{2})}\rangle_{Av}=0.35$; $\langle I_{(11\bar{3})}\rangle_{Av}=0.18$.

The values of $I_{(22\bar{2})}$ can be computed for points along the $(22\bar{2})$ zone boundary other than the corners (Appendix II). $I_{(22\bar{2})}$ will generally decrease upon leaving a corner and moving along the $(22\bar{2})$ boundary. A strong $(22\bar{2})$ reflection is thus obtained only from restricted regions of the $(22\bar{2})$ boundary.

Having investigated the behavior at zone corners formed by Brillouin zone boundaries, one of which has a zero structure factor, the question arises as to the behavior at a corner where both structure

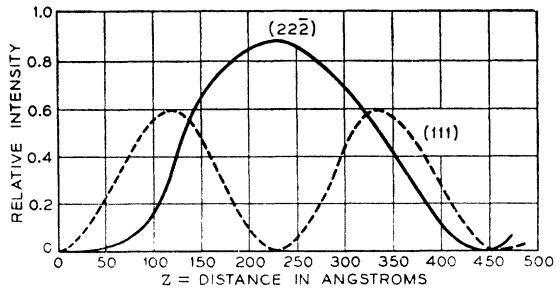

FIG. 7. Intensities of the (111) and (22$\bar{2}$) reflections as a function of depth of penetration in crystal. Incident crystal wave vector terminates at (111)|(22$\bar{2}$) boundary (point C, Fig. 6). Amplitude of (11$\bar{3}$) reflection neglected. The (222) intensity builds up more slowly than the (111). 40-kv electrons, $\lambda=0.061$A.

factors are non-zero. Point F (Fig. 6) or the (331)|(113) corner will serve as an example. Here $s\equiv(331)$, $g(113)$ and $\lambda=(22\bar{2})$. Since $v_\lambda=0$ and $|K_\lambda|^2>|K_0|^2$, the amplitude coefficient C_λ can be neglected. The intensities are found to be

$$I_{(113)}=0.77\sin^2\pi z/z_0 \text{ with } z_0=\lambda E/\Delta E;$$
$$\Delta E=(|v_g|^2+|v_s|^2)^{\frac{1}{2}},$$
$$I_{(331)}=0.23\sin^2 z/z_0.$$

Both intensities possess the period $z_0=\lambda E/\Delta E$ in contrast to the mixed periods found at points A, B, C, and D. The reason lies in the matrix since the root $\beta_0{}^0=0$ requires $C_0{}^0=0$. There are thus only two incident crystal wave vectors, $K_0{}^1$ and $K_0{}^2$. If K_0 moves away from the corner (331)|(113) along the (113) boundary, $I_{(113)}$ becomes

$$I_{(113)}=\sin^2\pi z/z_0 \text{ with } z_0=\lambda E/(V_{113}).$$

Along the (331) boundary away from the corner,

$$I_{(331)}=\sin^2 z/z_0 \text{ with } z_0=\lambda E/(v_{331}).$$

Thus, at the corner, not only is the intensity partitioned between the two diffracted beams, but the period z_0 is reduced to a lower value than it would be for either reflection alone. This suggests that the values of z_0 measured from electron micrographs of regular crystals [3,9] should be interpreted cautiously. In the case of MgO crystals, the calculated value of $z_0{}^i$ is 410A for the (200) reflection. The value measured by Hall[9] is about 300A (although an observed value of 420A was reported by the author,[3] it has since been found that an error was made in the measurement and the value in this case is also about 300A). It seems likely that for the orientation of electron beam and MgO crystal at which the effect is observed, the incident crystal wave vector is near the (200)|(220) corner. In this case $z_0=320$A for 60-kv electrons or a value much nearer the experimental value than the 410A. Thus, in interpreting experimental observations on the basis of the dynamical theory, it now appears that the simple results for only one diffracted beam may often be inadequate.

Only a fraction of the Brillouin zone edges involving the (222) boundaries have been considered. The ones shown in Fig. 6 are typical but not complete even for the (22$\bar{2}$) boundary. The (33$\bar{1}$)|(22$\bar{2}$) boundary occurs between A and B, for example, and couples with ($\bar{1}\bar{1}1$).

If the structure factors for two of the indices satisfying the relation $\lambda=s-g$ are zero, a "forbidden" reflection does not occur. For example, if $s\equiv(22\bar{2})$, $g\equiv(220)$, and $\lambda\equiv(00\bar{2})$, a step matrix results

$$\begin{pmatrix} \beta_0 & -v_g^* & 0 & 0 \\ -v_g & \beta_g & 0 & 0 \\ 0 & 0 & \beta_s & -v_g \\ 0 & 0 & -v_g^* & \beta_\lambda \end{pmatrix}$$

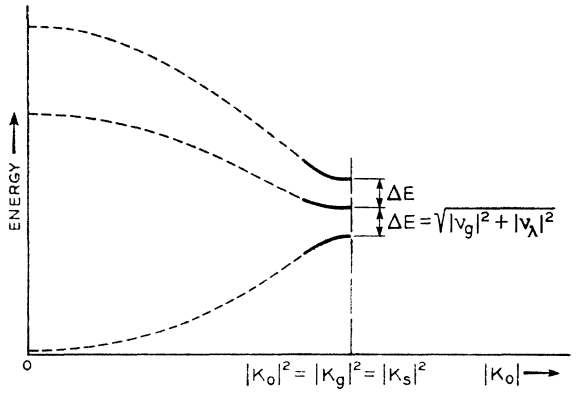

FIG. 8. Plot of energy $vs.$ incident wave number $|K_0|$ along the wave vector K_0 to the (111)|(22$\bar{2}$) Brillouin zone edge in the reduced zone scheme. C_λ is neglected here to yield the cubic approximation (Eq. (23)). The solid portions of the curves are calculated from (23) while the dotted regions are schematic since the solutions hold only in the neighborhood of a zone edge. For this case, $\Delta E=10.5$ volts.

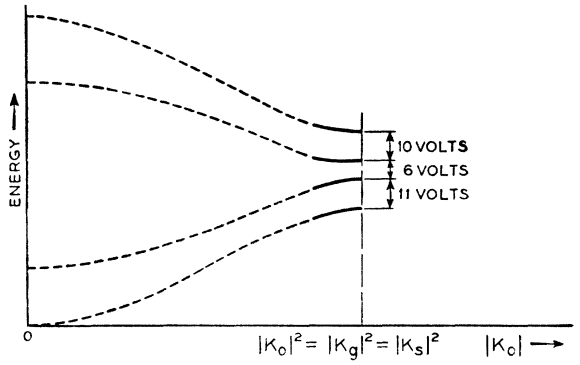

FIG. 9. Plot similar to Fig. 8 for the (111)|(22$\bar{2}$) zone corner with C_λ not neglected yielding the quartic approximation (Eq. (24)). The quadratic approximation (Fig. 2 of reference 1) gives two distinct energy levels and a single gap far from a zone edge. The cubic approximation at an edge results in three levels and two gaps while the quartic gives four levels and three gaps. The perturbation increases as the order of approximation increases.

[9] C. E. Hall, J. App. Phys. 19, 198 (1948).
Using the quadratic approximation (reference 3).

and the only reflection that will occur is (220) since there is no perturbation at the (220)|(22$\bar{2}$) corner.

The dynamical theory seems to be at least in semiquantitative agreement with experimental observations on the intensity of the (222) Laue spot obtained from single crystals of silicon and germanium. As previously mentioned, for certain settings of the crystal, the strongest spot in the pattern is found to be the (222). This is evidently possible when the incident crystal wave vector terminates at the corner formed by the (222) Brillouin zone boundary and another boundary such as (111), (113), or (331). In the case of a powder pattern (Debye-Scherrer rings), such as Fig. 2(b), it is difficult to predict the (222) intensity averaged over all orientations.[j] An idea as to the procedure necessary to obtain an average intensity for a perturbation reflection can be obtained from Fig. 10. Figure 10 shows the (222) Brillouin zone boundary for the diamond lattice. The dark shaded lines are the neighborhoods of the intersections of Brillouin zone boundaries of the form (111), (113), and (331) with the (222) boundary and represent the regions in which the perturbation (222) reflection will result.[k] On the basis of the network analogy, the dark regions are those in which there is effective coupling to the (222) mesh while in the white region the (222) mesh is isolated. For lack of any other name, the dark region of Fig. 10 will be called a "perturbation (or coupling) grid." The total perturbation grid extends over all faces of the (222) octahedron. (The octahedron so formed is not strictly a Brillouin zone as the term is used in solid state physics. It might be termed a "pure zone," however, since all faces have indices of the same form, i.e., (222), ($\bar{2}\bar{2}\bar{2}$), (22$\bar{2}$), etc. for this case.) The average intensity of a (222) Debye-Scherrer ring is then obtained by averaging over the entire (222) octahedron. The fraction of the total area of a pure zone occupied by the perturbation grid would be a rough measure of the average intensity of a Debye-Scherrer ring. In Appendix II it is shown that the widths of the grid lines are of the order of 2°.

Having demonstrated that a (222) reflection is to be expected from the diamond lattice, the question arises as to whether or not other perturbation reflections may not arise in the same way. For example, the (200) structure factor for diamond is also zero. Calculations for several corners ((002)|(33$\bar{1}$), (002)|(111), (002)|(113), and (002)|(331)) have been made and indicate that a strong (002) should occur at these corners and others. Diffraction patterns from evaporated germanium and silicon generally show a weak (200) ring but a strong Laue spot from a single crystal has not been reported. With a suitably oriented crystal, a strong (200) reflection should be obtained if the theory is correct. The multiplicity for (200) is six as compared to eight for (222) which reduces the change of finding the correct orientation in randomly oriented crystals. An experiment to find the (200) Laue spot seems called for.

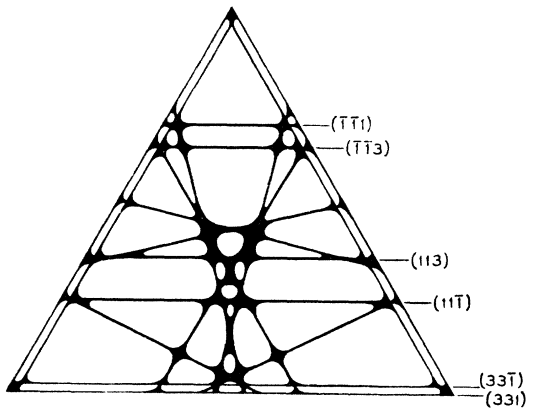

FIG. 10. View normal to the (22$\bar{2}$) Brillouin zone face of the (222) octahedron in reciprocal space. The array of intersecting lines consists of zone edges formed by intersections of the (22$\bar{2}$) face with other zone boundaries and is termed a "perturbation grid." The widths of the grid lines are of the order of a degree or so (Appendix II) with increased broadening near intersections as shown schematically above. The perturbation grid extends over all faces of the octahedron.

A perturbation grid occurs for all zone boundaries in any crystal whether or not the structure factor vanishes. If the structure factor is not zero, then the effect of the perturbation grid is not so evident since an appreciable change in intensity from that expected with the kinematic theory is unlikely and would be difficult to detect experimentally due to complications arising from factors such as preferred orientation, distortion, etc. Cases in which the structure factor is zero should be the most fruitful in this type application of the dynamical theory.

IV. GENERAL REMARKS

The presence of the (222) reflection in electron diffraction patterns of elements possessing the diamond structure seems at present to be adequately explained by the dynamical theory. Experimental verification[2,3,9] of the approximate correctness of several of the salient features of the dynamical theory leads to a reasonable amount of confidence in the foregoing explanation of the (222) reflection. The general approach and treatment is not unique to electrons, however, and could be carried out for x-rays as well.* The case of a single diffracted beam in x-ray diffraction was worked out some thirty

[j] For the case of only one strong diffracted beam, the integration has been carried out to obtain the intensities of Debye-Scherrer rings. M. Blackman, Proc. Roy. Soc. (London) **A174**, 68 (1939).

[k] See Appendix II for calculations pertaining to the width of the lines.

* See J. Weigle and H. Müksam, Helv. Phys. Acta. **10**, 139 (1937).

years ago by Darwin and Ewald.[10] The transition to the x-ray case can be readily accomplished by noting that the quantity $|v_g|/E$ occuring in the argument of the $\sin^2$ term for the simple electron case becomes $(K/(|\gamma_0\gamma_g|)^{\frac{1}{2}})|\sigma_g|$ for x-rays,[10] where $K=1$ for normal polarization, σ_g is the polarizability coefficient, and γ_0, γ_g are the direction cosines for the incident and diffracted beams, respectively. If α denotes the polarizability, then

$$\sigma \equiv 4\pi\alpha = \sum_g \sigma_g e^{2\pi i(g\cdot r)}$$

(the x-ray counter part of Eq. (4)) and

$$|\sigma_g| = (e^2\lambda^2/m\pi^2\Omega)|F_g|,$$

e is the electronic charge, λ the wave-length, m the electron mass, c the ratio of the electrostatic and electromagnetic units, Ω the volume of the unit cell, and F_g the x-ray structure factor. For the case when the Ewald sphere touches reciprocal lattice points (111) and $(22\bar{2})$, Eqs. (22a) may be applied with

$$z_0 \simeq \frac{2\lambda}{(|\sigma_g|^2+|\sigma|^2)^{\frac{1}{2}}} = 1.44\times10^{-4} \text{ cm for } \lambda = 1.5\text{A}.$$

The two cases, electron and x-ray, thus differ only by a change of scale as can be seen. The x-ray $(22\bar{2})$ reflection does not reach maximum intensity until the depth of penetration is about 8000A in germanium as compared to 225A in the electron case. From the equivalent circuit point of view, the couplings in the x-ray case are much weaker than in the electron case.

The period $z_0 \simeq 1.4\times10^{-4}$ cm (in germanium) for 1.5A x-rays is of the same order as the estimates of mosaic size. If the coherent path length in a crystal is l, then the relative intensity of a reflection will be dependent upon l. In the case of diamond, z_0 is about 4×10^{-4} cm for the (222) and the intensity should be sensitive to the mosaic size of the crystal. This appears to be in qualitative agreement with experimental observation.[11] However, the dependence of intensity upon mosaic size does not require that the x-ray (222) in diamond originate primarily through the perturbation grid on the (222) octahedron (Fig. 10). The simple case for only a single diffracted beam wherein the (222) structure factor is not zero (due to valence electron distribution) would also predict a dependence of intensity upon coherent path length. The width of the perturbation grid lines for the x-ray case will be of the order of about one-fifth of those for the electron case according to a rough calculation. The region in which a perturbation (222) can occur in the x-ray case is then smaller than for the electron case. It would appear desirable to carry through the perturbation calculation in detail for the x-ray case in an effort to determine whether or not the dynamical theory alone is sufficient to account for the (222).

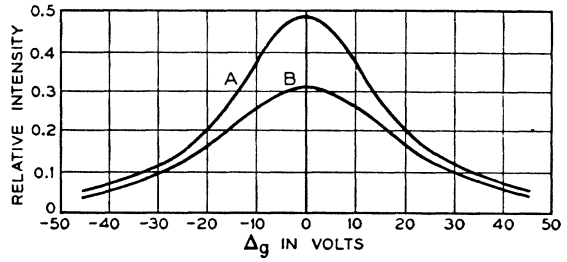

FIG. 11. Rocking curves for the Ge (111) reflection averaged over thickness showing the difference in width far from a Brillouin zone edge, A, and at the $(111)|(22\bar{2})$ edge, B. Curve A is the quadratic approximation for only one diffracted beam. Curve B is the cubic approximation with the incident wave vector maintaining its terminus on the $(22\bar{2})$ boundary and running either direction away from the $(111)|(22\bar{2})$ edge. The deviation from the Laue condition, Δg, is given in volts which can be converted to radians, $\Delta\theta$, through the relation $\Delta\theta=\Delta_g d/2E\lambda$ where d is the interplanar spacing, E the total energy, and λ the wave-length. For 40-kv electrons, $\Delta\theta=1.3\times10^{-3}\Delta g$.

[10] See W. Zachariasen, *Theory of X-ray, Diffraction in Crystals* (John Wiley and Sons, Inc., New York, 1945), Sections 3, 8–11.

I am indebted to various members of the technical staff for aid and criticism and particularly to Dr. C. Herring for help in developing the general theory and to Dr. R. L. Dietzold for aid in the equivalent circuit treatment.

APPENDIX I. FOURIER COEFFICIENTS

The Fourier coefficients of potentials are given by†

$$v_g = (e/\pi\Omega|g|^2)\Sigma_j (Z_j - f_j)\exp[2\pi i(g_j\cdot r_j)] \text{ e.s.u.} \quad \text{(I-1)}$$

and $v_{hkl}(\text{volts}) = 300\, v_g$. Ω is the volume of the unit cell.

Some of the coefficients for germanium used in the text are displayed below and were calculated using formula (I-1).

Germanium:	Silicon:	Diamond:
$a_0=5.65$A	$a_0=5.42$A	$a_0=3.56$A
$\Omega=180$A^3	$\Omega=159$A^3	$\Omega=45$A^3.

The unit cells contain eight atoms with the basis

(000), $(\frac{1}{2}\frac{1}{2}0)$, $(\frac{1}{2}0\frac{1}{2})$, $(0\frac{1}{2}\frac{1}{2})$, $(\frac{1}{4}\frac{1}{4}\frac{1}{4})$, $(\frac{3}{4}\frac{3}{4}\frac{1}{4})$, $(\frac{1}{4}\frac{3}{4}\frac{3}{4})$, $(\frac{3}{4}\frac{1}{4}\frac{3}{4})$.

Germanium:

hkl	(111)	$(11\bar{1})$	$(\bar{1}\bar{1}\bar{1})$	(113)
v_{hkl}	$6(1-i)$	$6(1+i)$	$6(1+i)$	$4.5(1-i)$
$\lvert v_{hkl}\rvert$	8.5 volts	8.5	8.5	6.4
hkl	$(11\bar{3})$	(331)	$(33\bar{1})$	$(11\bar{5})$
v_{hkl}	$4.5(1-i)$	$2.5(1-i)$	$2.5(1+i)$	$1.9(1+i)$
$\lvert v_{hkl}\rvert$	6.4	3.5	3.5	2.7

APPENDIX II. ROCKING CURVES

The behavior of the diffracted intensities in the neighborhood of a Brillouin zone corner is important in considering

[11] Robertson, Fox, and Martin, Phil. Trans. **A232**, 474 (1934).

† The deviation, Δ_g, can be converted to radians through the relation $\Delta\theta=\Delta_g d/2E_\lambda$ where d is the interplanar spacing.

the widths of the perturbation grid lines of Fig. 10. A calculation of the intensities as a function of the deviation, Δg from the Laue condition is required and can be carried out readily for the cubic approximation. For corner C (Fig. 6, the (111)|(22$\bar{2}$) corner) the matrix (15) becomes

$$\begin{pmatrix} \beta_0 & -v_g^* & 0 \\ -v_g & \beta_0+\Delta_g & -v_\lambda^* \\ 0 & -v_\lambda & \beta_0 \end{pmatrix}, \quad \begin{matrix} g\equiv(111) \\ s\equiv(22\bar{2}) \\ \lambda\equiv(11\bar{3}) \end{matrix} \qquad \text{(II-1)}$$

where $\Delta_g\equiv(h^2/8\pi^2m)(|K_g|^2-|K_0|^2)$ is the deviation from the Laue condition for the wave vector Kg. In this $\Delta_s=0$ since K_0 is to maintain its terminus on the (22$\bar{2}$) zone boundary but may move away from the corner in either direction. The secular determinant of (II-1) yields the roots

$$\begin{aligned} \beta_0^0&=0, \\ \beta_0^1&=-(\Delta_g/2)+[(\Delta_g/2)^2+(\Delta E)^2]^{\frac{1}{2}}, \\ \beta_0^2&=-(\Delta_g/2)-[(\Delta_g/2)^2+(\Delta E)^2]^{\frac{1}{2}}, \end{aligned}$$

with $\Delta E=(|v_g|^2+|v_\lambda|^2)^{\frac{1}{2}}$ as before (Fig. 8). Using the roots (II-2), the beat wave vectors are found to be

$$\begin{aligned} \Delta K_{01}&=K_0^1-K_0^0=(\pi/\lambda E^{(0)})\{-(\Delta_g/2)+[(\Delta_g/2)^2+(\Delta E)^2]^{\frac{1}{2}}\}, \\ \Delta K_{02}&=K_0^2-K_0^0=(\pi/\lambda E^{(0)})\{-(\Delta_g/2)-[(\Delta_g/2)^2+(\Delta E)^2]^{\frac{1}{2}}\}, \\ \Delta K_{12}&=K_0^2-K_0^1=(-2\pi/\lambda E^{(0)})[(\Delta_g/2)^2+(\Delta E)^2]^{\frac{1}{2}}. \end{aligned} \qquad \text{(II-3)}$$

The ratios of the amplitude coefficients $\alpha_g=C_g/C_0$, etc. are now

$$\alpha_g^0=0,$$

$$\alpha_g^1=\frac{1}{v_g^*}\left\{-\frac{\Delta_g}{2}+\left[\left(\frac{\Delta_g}{2}\right)^2+(\Delta E)^2\right]^{\frac{1}{2}}\right\}, \quad \alpha_s^0=-\frac{v_g}{v_\lambda^*},$$

$$\alpha_g^2=\frac{1}{v_g^*}\left\{-\frac{\Delta_g}{2}-\left[\left(\frac{\Delta_g}{2}\right)^2+(\Delta E)^2\right]^{\frac{1}{2}}\right\}, \quad \alpha_s^1=\alpha_s^2=\frac{v_\lambda}{v_g^*}, \qquad \text{(II-4)}$$

in contrast to Eq. (20). From (14b) and (21) the diffracted intensities are found to be

$$\begin{aligned} I_{(222)}=&\frac{|\alpha_s^0|^2|\alpha_s^1|^2}{|\alpha_s^1-\alpha_s^0|^2|\alpha_g^2-\alpha_g^1|^2}[4(|\alpha_g^2|^2-\alpha_g^{2*}\alpha_g^1) \\ &\times\sin^2\tfrac{1}{2}\Delta K_{01}z+4(|\alpha_g^1|^2-\alpha_g^2\alpha_g^{1*})\sin^2\tfrac{1}{2}\Delta K_{02}z \\ &+2(\alpha_g^2\alpha_g^{1*}+\alpha_g^{2*}\alpha_g^1)\sin^2\tfrac{1}{2}\Delta K_{12}z], \end{aligned} \qquad \text{(II-5)}$$

$$\begin{aligned} I_{(111)}=&4\frac{|\alpha_s^0|^2|\alpha_g^2|^2|\alpha_g^1|^2}{|\alpha_s^1-\alpha_s^0|^2|\alpha_g^2-\alpha_g^1|^2}\sin^2\tfrac{1}{2}\Delta K_{12}z \\ =&\frac{|v_g|^2}{(\Delta_g/2)^2+(\Delta E)^2}\sin^2\tfrac{1}{2}\Delta K_{12}z, \end{aligned}$$

in place of Eqs. (22a).

It is of interest to consider first the (111) intensity as given by (II-5). If $v_\lambda=v_{113}$ is neglected, $I_{(111)}$ reduces to the case for only one diffracted wave (reference 1) since now $(\Delta E)^2=|v_g|^2$ with

$$\Delta_g\equiv\frac{h^2}{8\pi^2m}(|K_g|^2-|K_0|^2)=2\frac{h^2}{8\pi^2n}|K|^2\Delta\theta\sin2\theta=2E^{(0)}\Delta\theta\sin2\theta,$$

where $\Delta\theta$ is the deviation from the Bragg angle θ. If the average value of $\sin^2=\frac{1}{2}$ is employed, the effect of thickness is eliminated and average rocking curves are obtained as shown in Fig. 11. The width at half-maximum intensity for the approximation of only one diffracted wave (far from a corner) is about 32 volts as compared to about 42 volts at the (111)|(22$\bar{2}$) corner. The width at half-maximum can be obtained directly from (II-5) as $[\Delta_g]_{\frac{1}{2}}=4\Delta E$ and is seen to be proportional to the energy gap at the zone boundary. The width of a Kikuchi line would then be greater for large energy gaps and hence greater if the incident wave vector terminates near a zone corner.

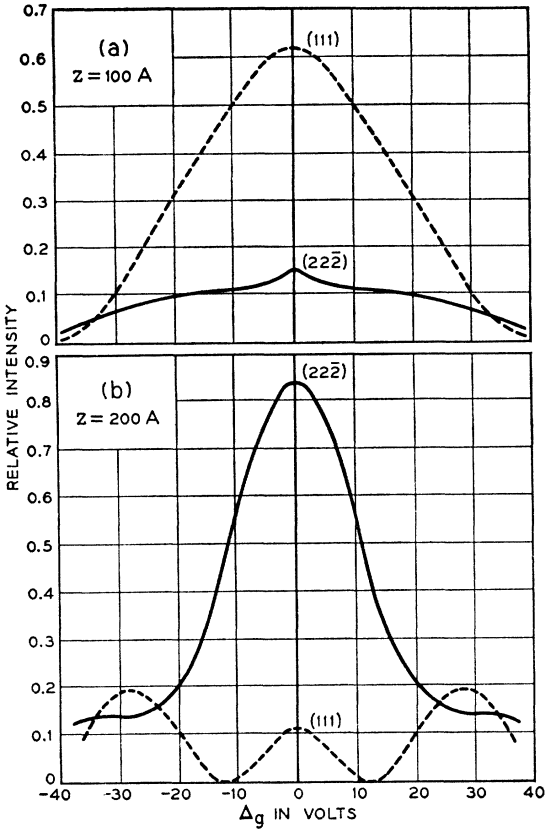

FIG. 12. Ge (111) and (22$\bar{2}$) rocking curves for two thicknesses of crystal as computed using the cubic approximation. The incident wave vector terminus is maintained on the (22$\bar{2}$) zone boundary and in the neighborhood of the (111)|(22$\bar{2}$) edge.

The width of the (222) reflection is not obtained quite as simply due to the presence of several periods in the expression (II-5) for the intensity. Equation (II-5) has been plotted for two different thicknesses, 100A and 200A, and is shown in Fig. 12. The (111) is also plotted for the same thickness for comparison. The subsidiary maxima are evident for the (111) reflection in Fig. 12(b) and are more intense than the primary. The half-widths of the (222) rocking curve from germanium are seen to be about 54 volts with a thickness of 100A and 26 volts at 200A. The (222) exhibits in both cases a greater half-width than does the (111). Experimentally, this should show up as a broader (222) Kikuchi line.

The half-widths of the grid lines of Fig. 10 are thus seen to be of the order of 5×10^{-2} rad. or about 2° for 40-kv electrons.

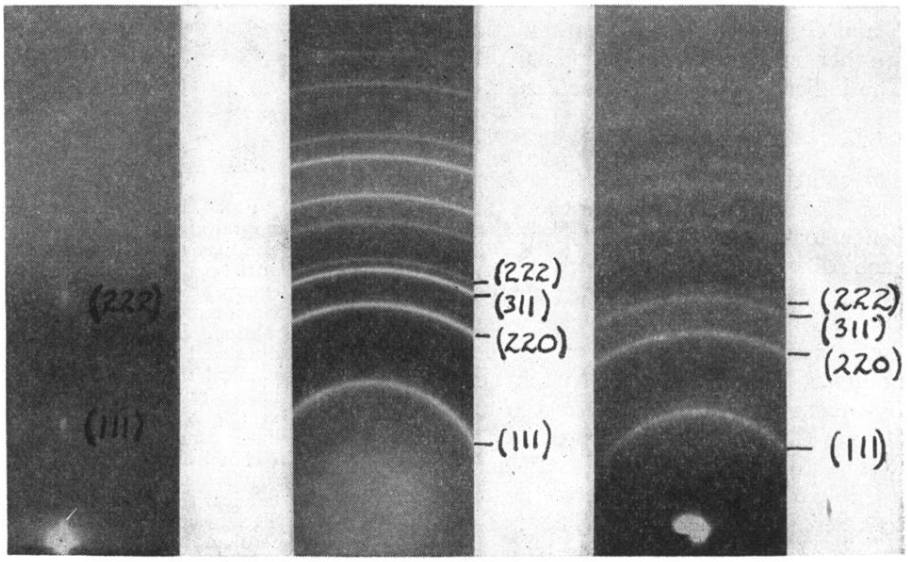

FIG. 2. Examples of the "forbidden" (222) reflection in electron diffraction patterns from silicon and germanium (40-kv electrons). (a) Strong (222) Laue spot from an etched single crystal of silicon. (Courtesy of K. H. Storks.) (b) Transmission pattern from an evaporated germanium film on a silica substrate. (c) Reflection pattern from a ground germanium surface showing grainy rings.